

Supplementary information

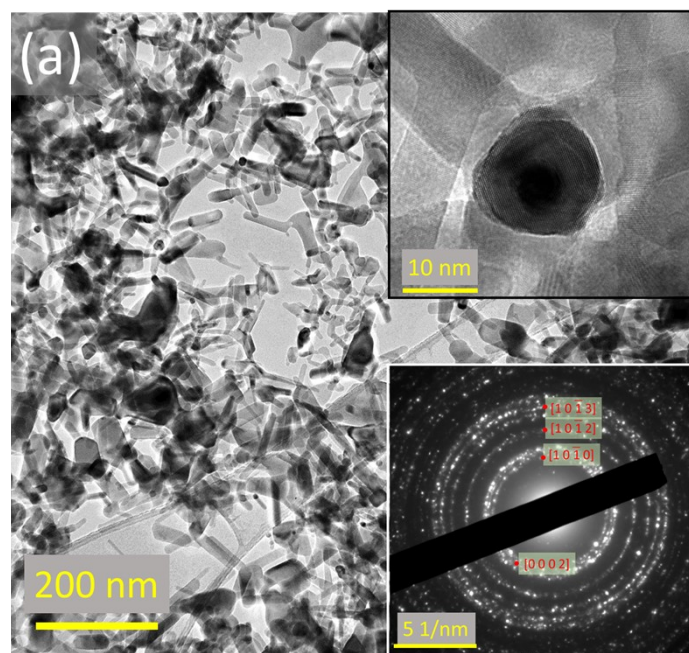
Non-equilibrium defect chemistry in oxygen-rich zinc oxide nano-tetrapods synthesized by atmospheric pressure microplasma.

Dilli babu Padmanaban, Paul Maguire and Davide Mariotti

School of Engineering, Ulster University, Belfast, BT15 1AP, UK.

E-mail: d.mariotti@ulster.ac.uk

1. Transmission electron microscopy:



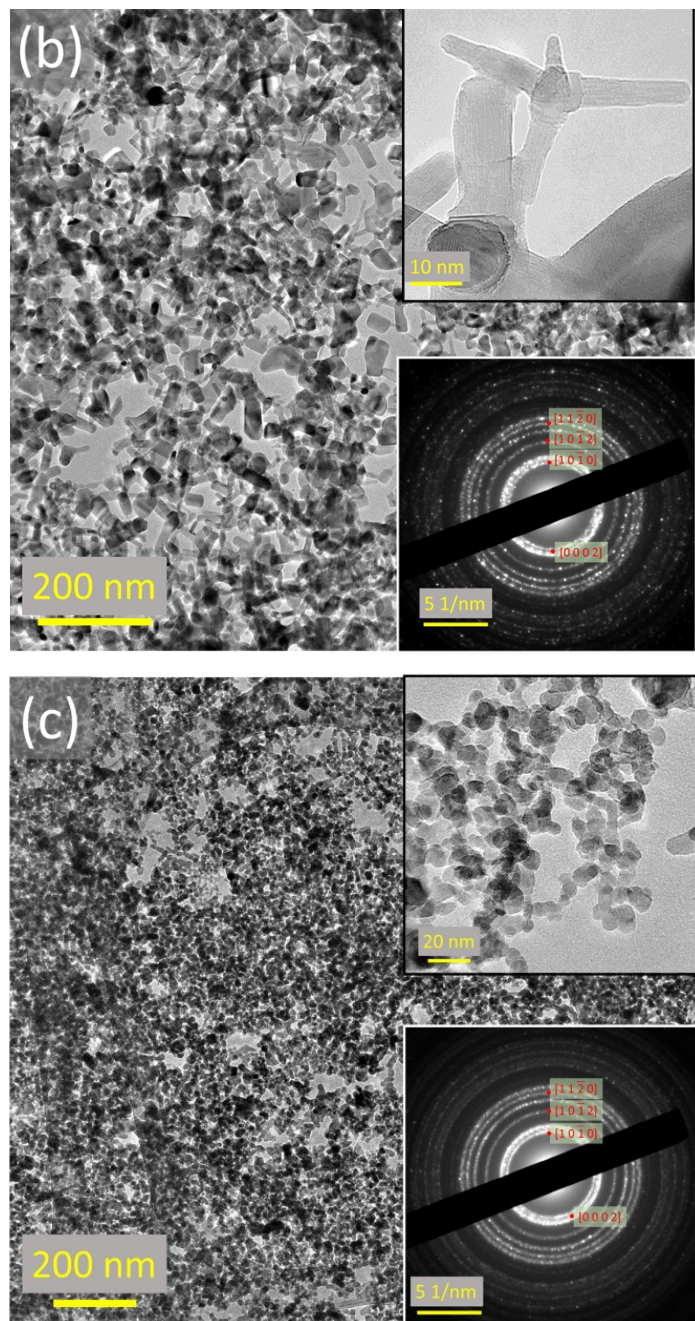


Figure S1. Transmission electron micrographs of ZnO nTPs and nanocrystals obtained for various He gas flows (a) 75 sccm, (b) 150 sccm and (c) 225 sccm for fixed 40 W RF power with inset of SAED pattern.

2. Optical properties

According to Tauc *et. al.*,^{1,2} absorption coefficient “ α ” of a material can be related to applied photon energy “ $h\nu$ ” in the form of equation 1, assuming the variation of $\alpha > 10^4 \text{ cm}^{-1}$

$$\alpha h\nu = A(h\nu - Eg)^r \quad (1)$$

where A is a constant and also called as band tailing parameter³, Eg is the bandgap and r represents the nature of the optical transition of the material. The latter can take values of $\frac{1}{2}$, 2, $\frac{3}{2}$ and 3 corresponding to allowed direct, allowed indirect, forbidden direct and forbidden indirect transitions respectively.²

The absorption coefficient (α) can be estimated using equation 2 (considering the scattering and reflection are negligible),

$$\alpha = \frac{1}{d} \ln T \text{ (cm}^{-1}) \quad (2)$$

where T is the measured light transmitted through a sample thickness d , i.e. path length, of the quartz cuvette used during measurement for various incident wavelengths.

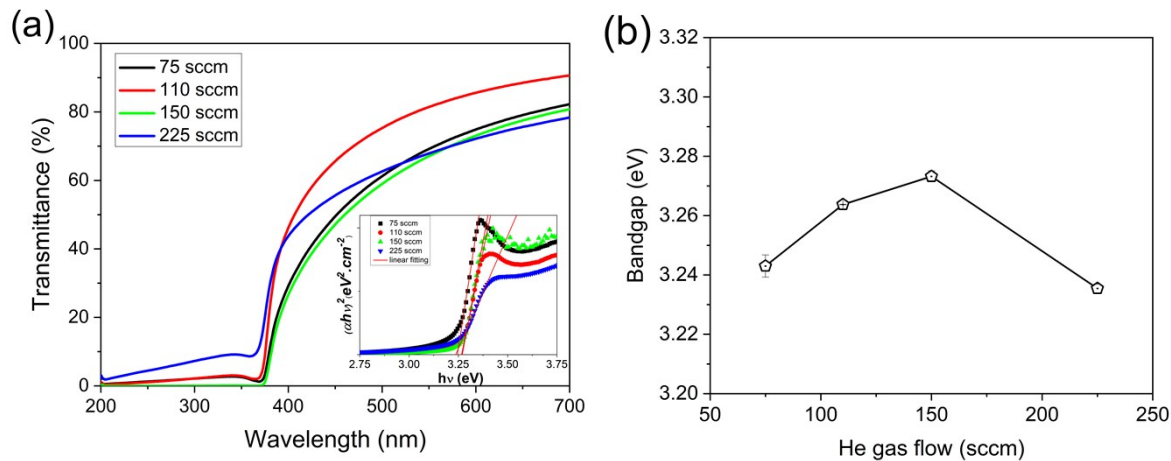


Figure S2. Optical transmittance of ZnO nTPs and nanoparticles for different gas flows: (a) light transmittance with corresponding Tauc's plots in the inset; whereas (b) variation of estimated bandgap observed for different He gas flows respectively.

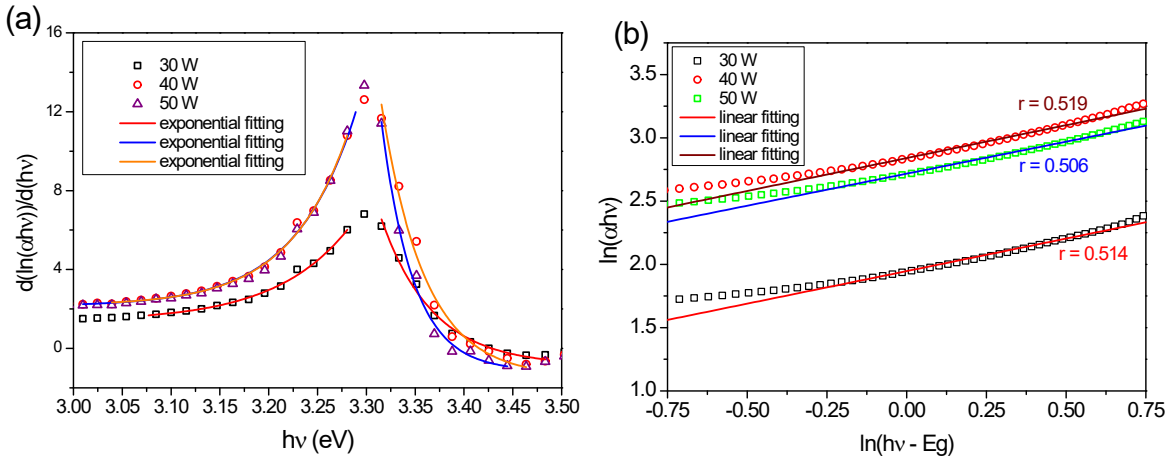


Figure S3. Plots showing (a) discontinuity at the band edge and (b) nature of transition obtained from light absorption for different wavelength from ZnO nTPs and nanoparticle obtained for different applied RF power.

The bandgap can be determined from a reported method² and equation 1 can re-writing as,

$$\frac{d\ln(\alpha h\nu)}{d(h\nu)} = \frac{r}{(h\nu - E_g)} \quad (3)$$

$$\ln(\alpha h\nu) = \ln(A) + r \ln(h\nu - E_g) \quad (4)$$

Equation 3, plotted as a function of $h\nu$, presents a discontinuity when the energy matches the bandgap (figure S3a). In this case the discontinuity occurs at 3.3 eV. Furthermore, the nature of the transition in terms of r can be determined by plotting $\ln(\alpha h\nu)$ vs $\ln(h\nu - E_g)$ (figure S3b) and by fitting the linear part reveals closest possible nature of transition; in this case this gives a value of $r = 0.49$, a close approximation that corresponds to a direct band transition ($r = \frac{1}{2}$).

We can now corroborate this finding by using the nature of the transition in a standard Tauc plot. We therefore use $r = 0.5$ to produce a Tauc plot (inset of figure 9a and S2a), which yields a bandgap of 3.26 eV (close to that of 3.3 eV previously determined).

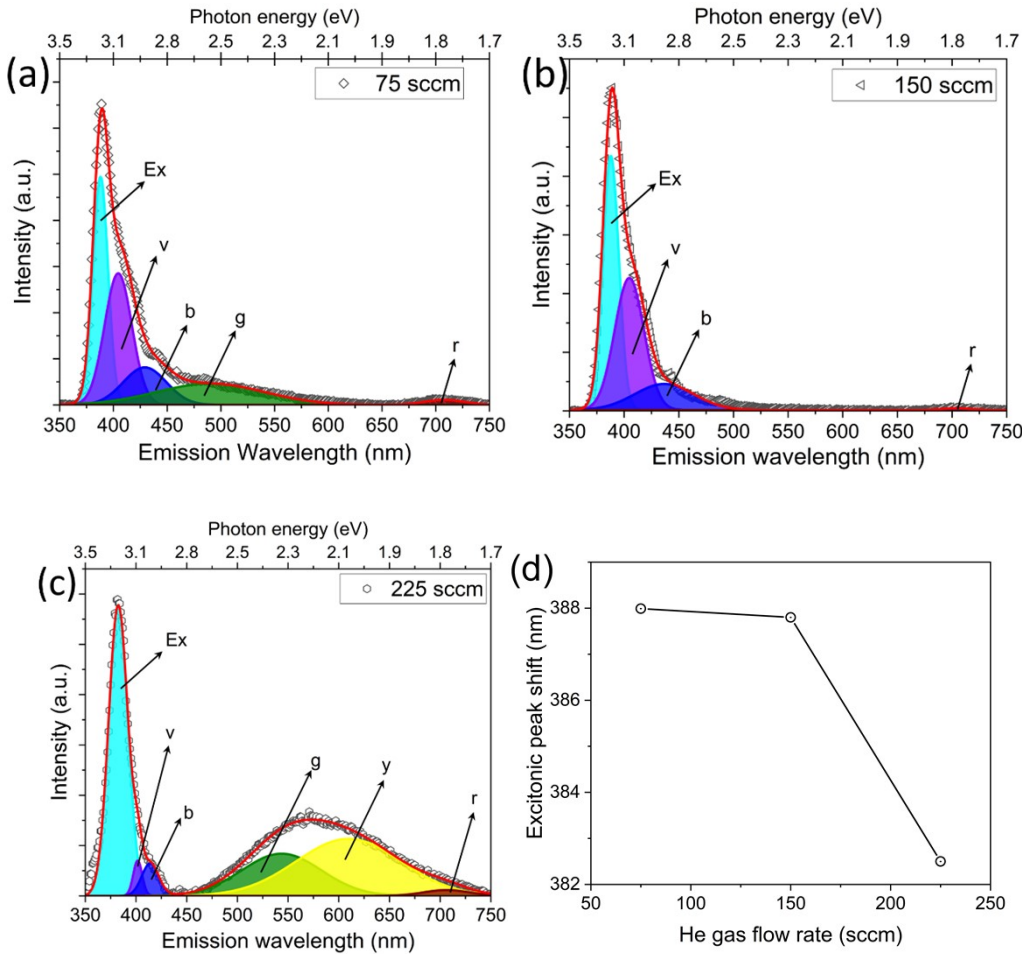


Figure S4 (a-c) Deconvoluted photoluminescence characteristics of ZnO NPs, whereas (d) variation of excitonic peak position for different He gas flows.

Table S1. List of photo emission peaks obtained from PL spectra at different He gas flows.

He gas flows (sccm)	<i>Interband emission, nm(eV)</i>	<i>Defect emission, nm(eV)</i>				
		<i>Ex</i>	<i>v</i>	<i>b</i>	<i>g</i>	<i>y</i>
75	387.99(3.20)	404.49(3.07)	429.22(2.89)	490.33(2.53)	-	707.97(1.75)
150	387.8(3.20)	404.71(3.06)	436.65(2.84)			704.11(1.76)
225	382.5(3.24)	401.67(3.09)	413.98(3.00)	543.6(2.28)	609.74(2.03)	706.44(1.76)

Table S2. Compilation of different emission bands and defect levels identified in PL of ZnO nanostructures and nanoparticles reported in literature.

Ref.	Inter-band emission or Near-band emission, or Free exciton combination (<i>Ex</i>)	Zinc deficient	Zinc rich	Oxygen deficient		Oxygen rich	
		Zn vacancy, (V _{zn})	Zn interstitial, (Zn _i)	Oxygen Vacancy, (V _o)		Oxygen interstitial, (O _i)	
		violet	blue	green	yellow	orange	red
⁴	380 - 390 nm	400 - 407 nm	432 - 437 nm	498-501 nm,	562 - 566 nm		
⁵	370-390 nm	~413 nm, 3 eV	~421 nm			~626 nm	640-650 nm
⁶	~381 nm (3.26 eV)				~577 nm (Vo*)	~640 nm	
⁷	~380 nm			~520 nm		~600 nm	
⁸	384-391 nm		421 nm	~520 nm (O _{zn})			
⁹	~380 nm			~490 nm		~580 nm	
¹⁰	~390 nm		~440 nm (interface traps)				
¹¹	~379nm						
¹²	~385 nm	~403 nm	428 nm(Zn _i), 450 nm(Zni ⁺)	495 nm (Vo ⁺), ~521 nm (O _{zn})	575 nm (Vo ⁺⁺)	~535 nm	
¹³	369-374 nm			~514 nm (Vo ⁺)			

3. X-ray Photoelectron Spectroscopy (XPS):

X-ray photoelectron spectroscopy (XPS) measurements were performed using a Kratos Axis Ultra DLD photoelectron spectrometer at $\approx 10^{-9}$ mbar base pressure. The survey and high-resolution spectra were acquired in high vacuum using a monochromatic Al K α X-ray radiation at 15 kV and 10 mA with analyser pass energy of 20 eV. The XPS sample is prepared by drop casting the colloidal samples on silicon substrates under ambient air at 60 °C. The acquired spectra are corrected for charge-shift using C 1s line at 284.6 eV.

The composition of the ZnO nTP crystal for 40 W, 110 sccm were analysed using XPS. Figure S4(a) shows the core-level spectra of zinc (Zn 2p) presents narrow doublets at 1021.1 eV and 1044.1 eV. The peaks were deconvoluted using an asymmetric Lorentzian function reveals Zn(II) in zinc oxide component at 1021.3 eV (reported at 1021.7 eV¹⁴) along with a minor component contributing for Zn (0) metallic zinc at 1020.9 eV. This can be presence of interstitial zinc atoms was also confirmed by XRD and photoluminescence emission. The broad O 1s core-level (figure S4(b)) was deconvoluted into two peaks. The first is at 529.7 eV, which is close to the reported value of 530.2¹⁵ and relates to lattice oxygen of zinc oxide. The second at 531.6 eV can be ascribed to oxygen vacancies (reported at 531.4¹⁶) or due to chemisorbed oxygen or hydroxyl or water molecule usually observed at further higher binding energy around 532 eV¹⁷.

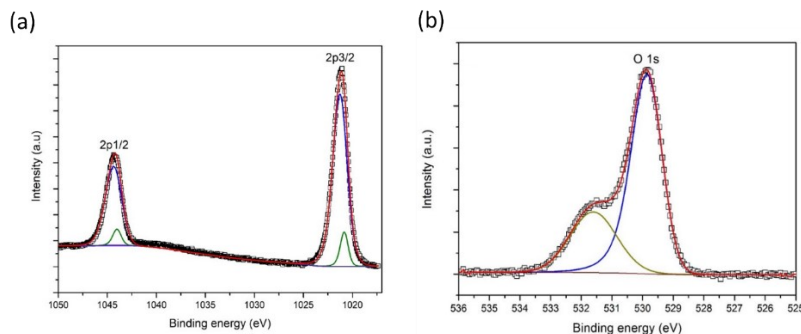
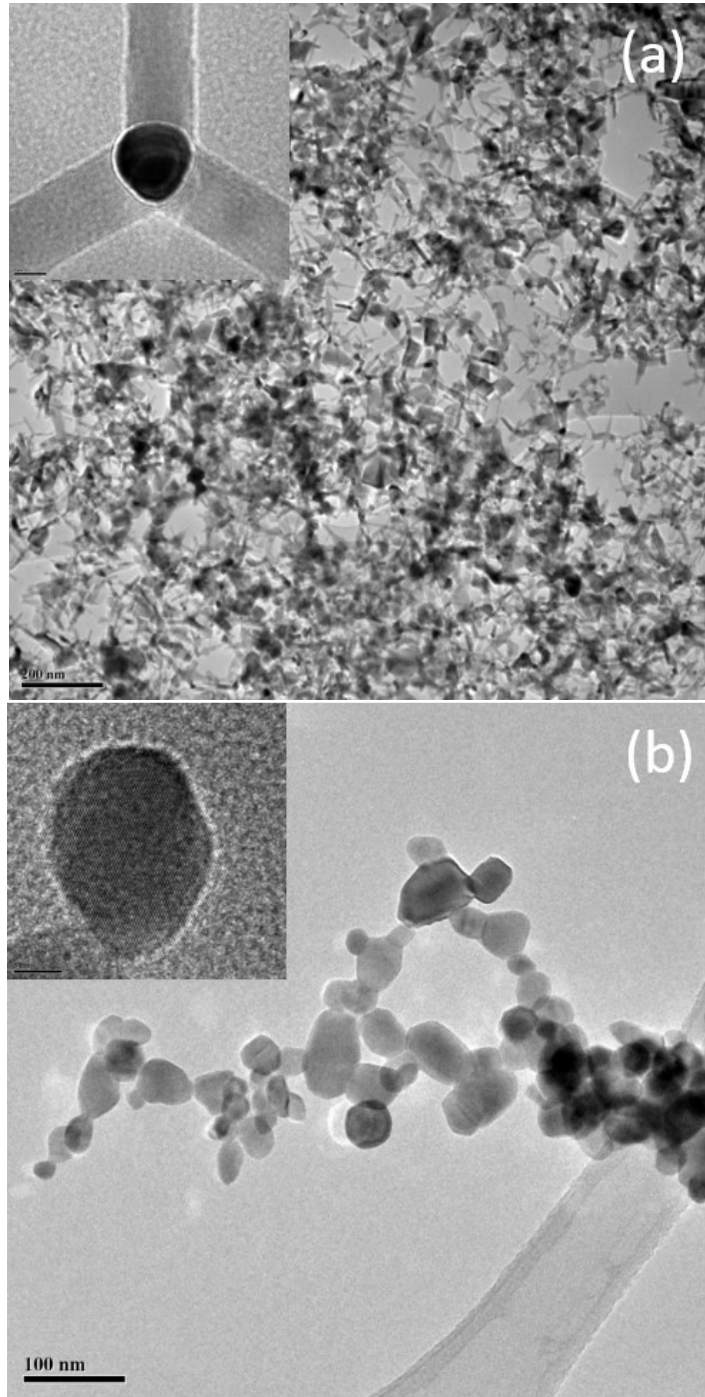


Figure S5. Core level spectra of (a) Zn 2p, and (b) O 1s.

4. Thermal stability of ZnO nTPs for different annealing temperature:

Transmission electron micrographs:



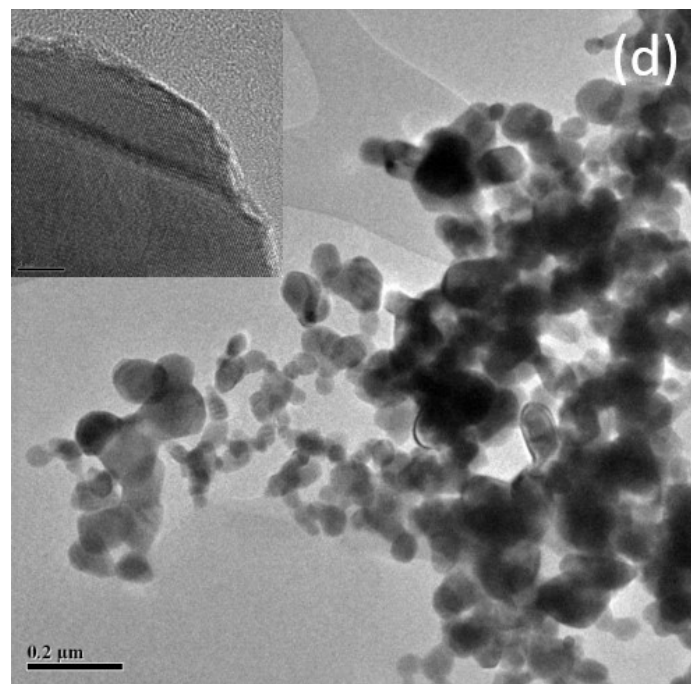
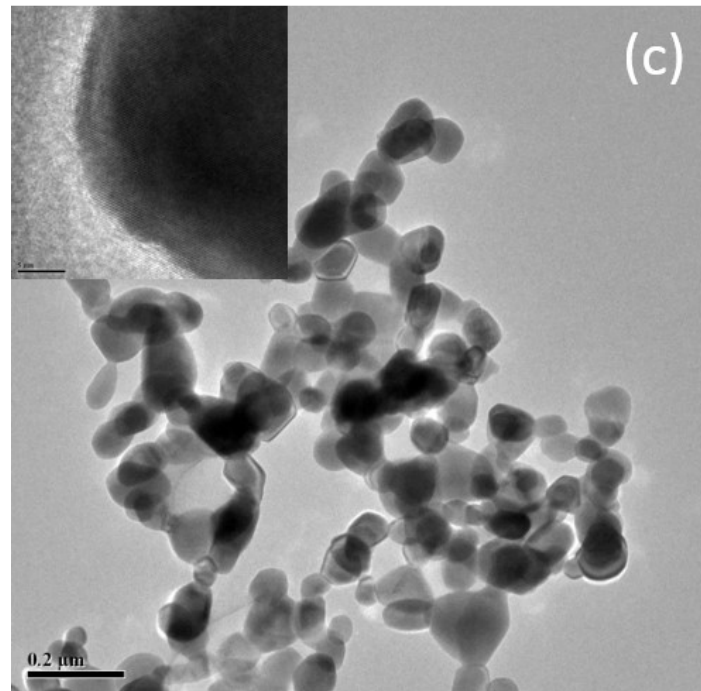


Figure S6. TEM micrograph of ZnO calcined at different temperature (a) as prepared nTP ZnO (b) 300 °C, (c) 500 °C and (d) 700 °C

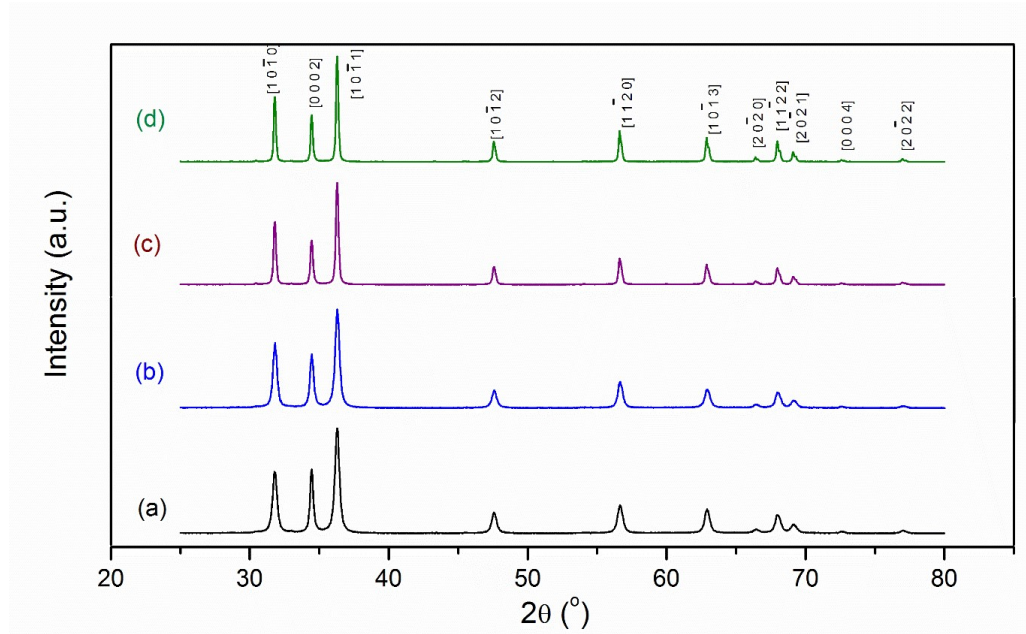


Figure S7. X-ray diffraction pattern of ZnO calcined at different temperature (a) as prepared nTP ZnO (b) 300 $^{\circ}$ C, (c) 500 $^{\circ}$ C and (d) 700 $^{\circ}$ C

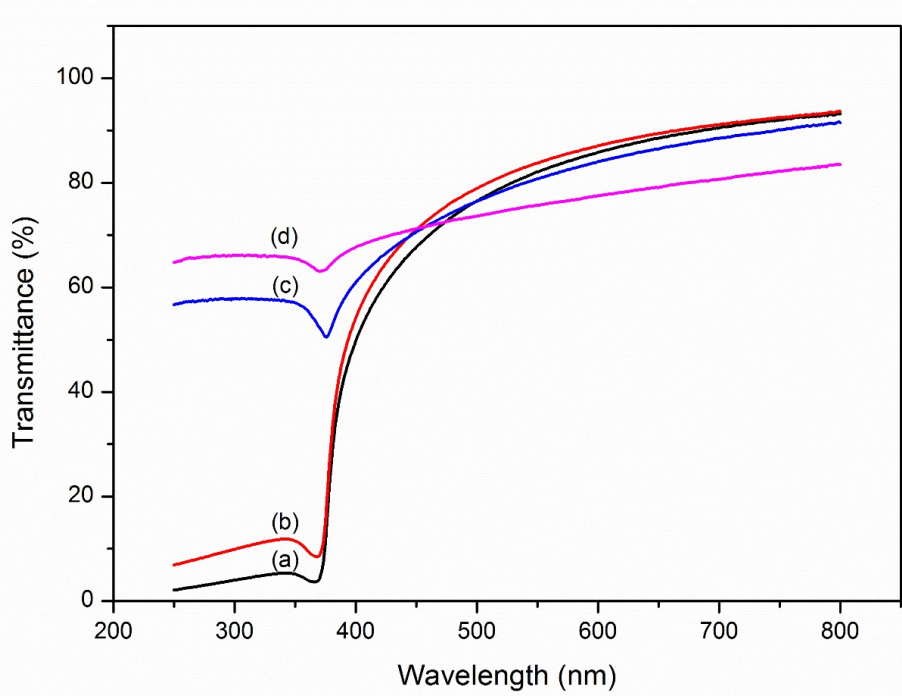


Figure S8. Transmittance measured by uv-vis spectroscopy of calcined ZnO at different temperature (a) as prepared nTP ZnO (b) 300 $^{\circ}$ C, (c) 500 $^{\circ}$ C and (d) 700 $^{\circ}$ C

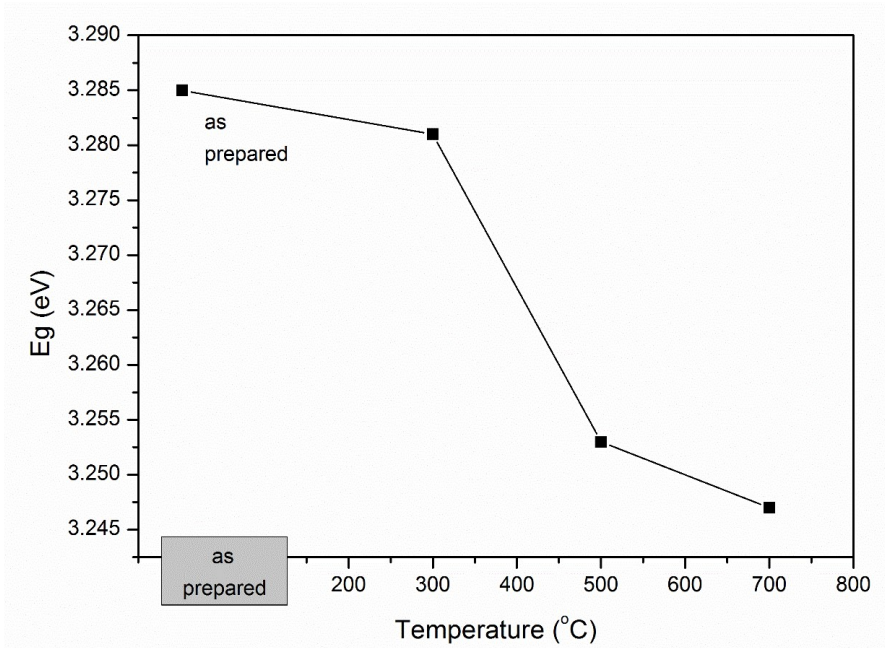


Figure S9. Variation of bandgap as calculated by Tauc plot for different calcination temperature.

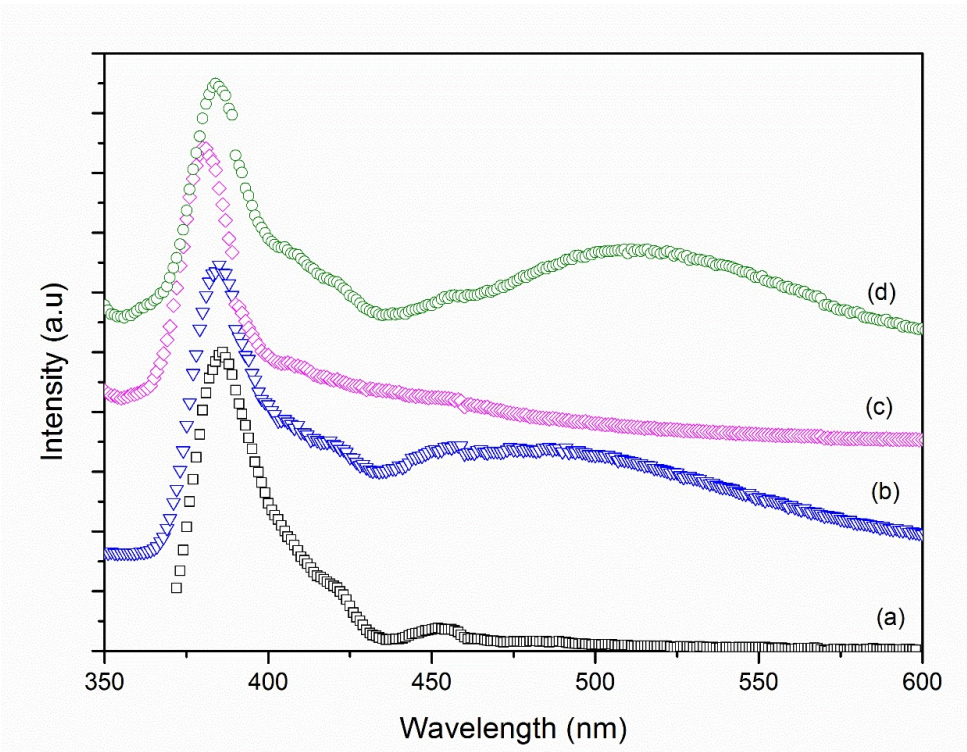


Figure S10. Photoluminescence emission spectra at 330 nm excitation of colloidal ZnO particle in ethanol (a) as prepared nTP ZnO (b) 300 °C, (c) 500 °C and (d) 700 °C

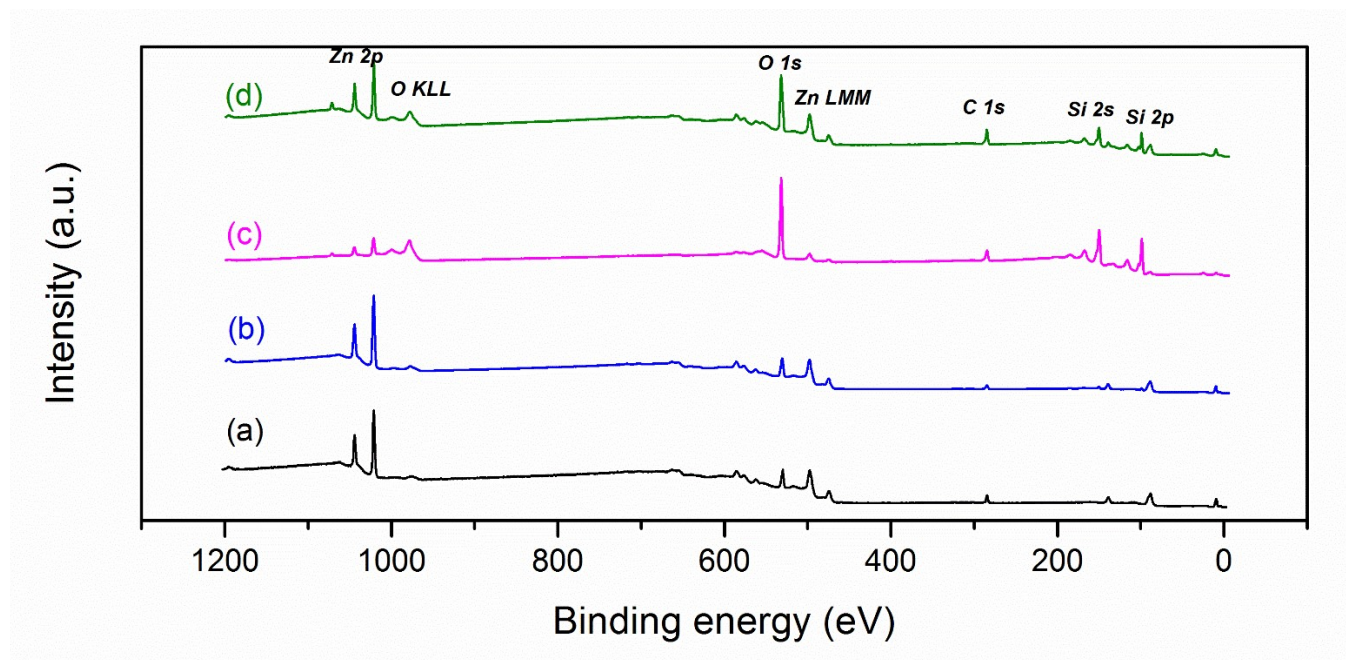


Figure S11. Survey scan spectra of ZnO nanoparticles on Si substrate for various calcination temperature (a) as prepared nTP ZnO (b) 300 °C, (c) 500 °C and (d) 700 °C

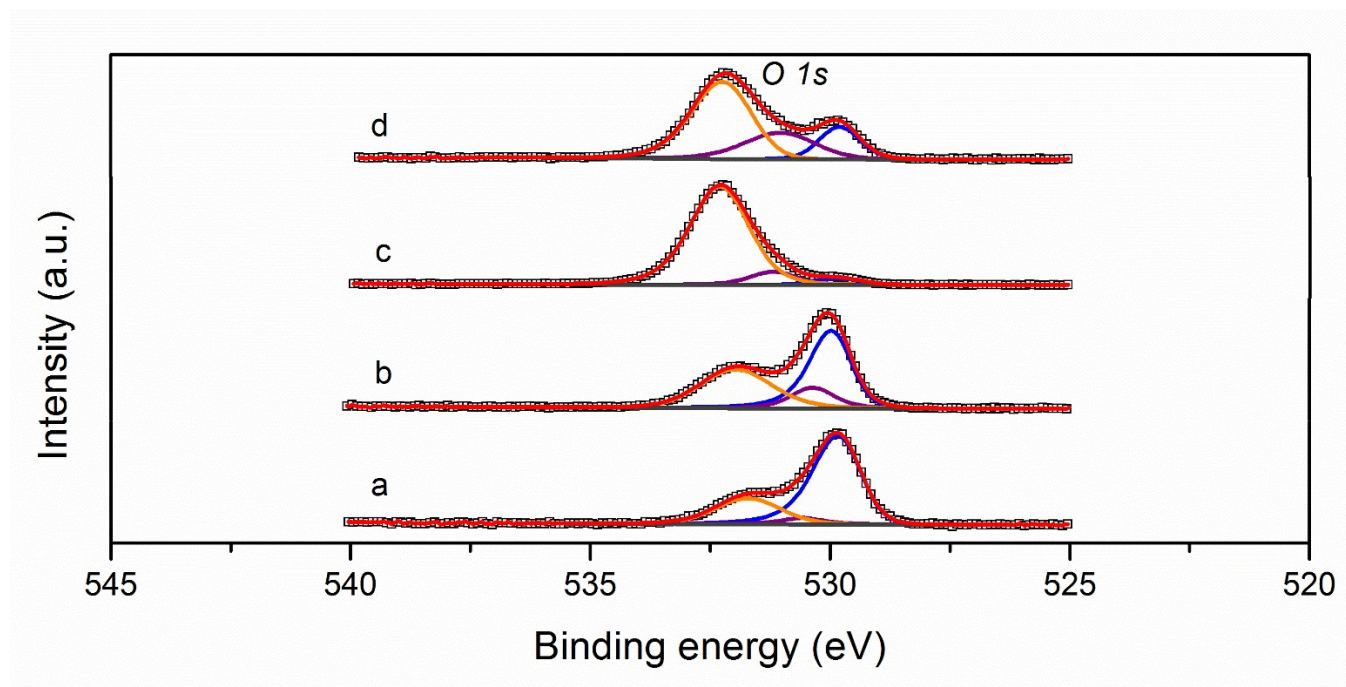


Figure S12. O 1s spectra of ZnO nanoparticles for various calcination temperature (a) as prepared nTP ZnO (b) 300 °C, (c) 500 °C and (d) 700 °C.

5. Comparison with other plasma processes:

Table S3. Compilation of different plasma synthesis of nanoscale ZnO morphologies including their process parameter reported in literature.

Reference	Plasma Setup	Operating Pressure	Plasma Source/Parameter	Gas	Precursor	Morphology/Size
<i>This work</i>	<i>Microplasma</i>	760 Torr (<i>Ambient</i>)	13.56 MHz Radio Frequency, 30 - 50 W	He	Zn wire	<i>Nanotrapods, Nanoparticles</i>
¹⁸	DC carbon arc Plasma	10 - 760 Torr	DC power, 10 - 200A	Air	Zn ingot	Nanoparticles, ~84 nm
¹⁹	Thermal plasma CVD	130 Torr	13.56 MHz Radio Frequency	Ar and O ₂	Zn solid	Nanocrystalline film
²⁰	Microwave plasma	~4 Torr	2.45 MHz Microwave, 400W	H ₂ , Ar, O ₂	Zn powder	Nanotubes, Nanowires, Nanocables
²¹	Plasma enhanced CVD	0.37-0.75 Torr	Radio Frequency, 20W	Ar and O ₂	Organometallic Zinc	1D-Nano-assemblies
²²	Plasma assisted MBE	~0.7 μTorr	13.56 MHz Radio Frequency,	O ₂	Zn metal	Nanotubes array
²³	Plasma pyrolysis	-	High frequency electric	Air	Zn salts	Nanoparticles, ~20 nm
^{24,25}	Solution plasma process	-	Pulsed DC, 450 V, 12 kHz		Zn salts	Nanospheres, ~17 nm
²⁶	DC plasma jet	~760 Torr (Atmospheric)	DC power, 7.5 kW	CO ₂ , Ar, and O ₂	Zn powder	Nanoparticles, Nanotrapods (Rod diameter = 20 ~100 nm)
²⁷	Soft jet plasma	~760 Torr (Atmospheric)	HV-AC power	Air	Zn salts	Nanomaterials
²⁸	RF thermal plasma	~760 Torr (Atmospheric)	Radio Frequency, 30 kW, 4 MHz	Ar, N ₂	Zn, ZnO powder	Nanorods, ~50 nm
²⁹	DC thermal plasma	~760 Torr (Atmospheric)	DC power, 70 kW	Air, Ar, and N ₂	Zn powder	Nanorods, D~30 nm, L~100-200 nm
³⁰	DC thermal plasma reactor	~760 Torr (Atmospheric)	DC power, 200 - 400 A	Ar and O ₂	Zn powder	Nanowires and Nanorods
³¹	Atmospheric pressure glow discharge	~760 Torr (<i>Ambient</i>)	13.56 MHz Radio Frequency,	He	Organometallic Zinc	Nanocrystals, 4-15 nm
³²	Solution precursor plasma spray	~760 Torr (<i>ambient</i>)	Arc current 600 A, 31.2 or 34.4 kW	Ar, H ₂	Organometallic Zinc	Nanostructure film
³³	Spray atomisation-assisted inductively coupled plasma	~760 Torr (<i>Ambient</i>)	13.56 MHz Radio frequency	Ar, O ₂	Zn salt	Nanoparticles, 17 - 26 nm

6. Additional electron microscopy images:

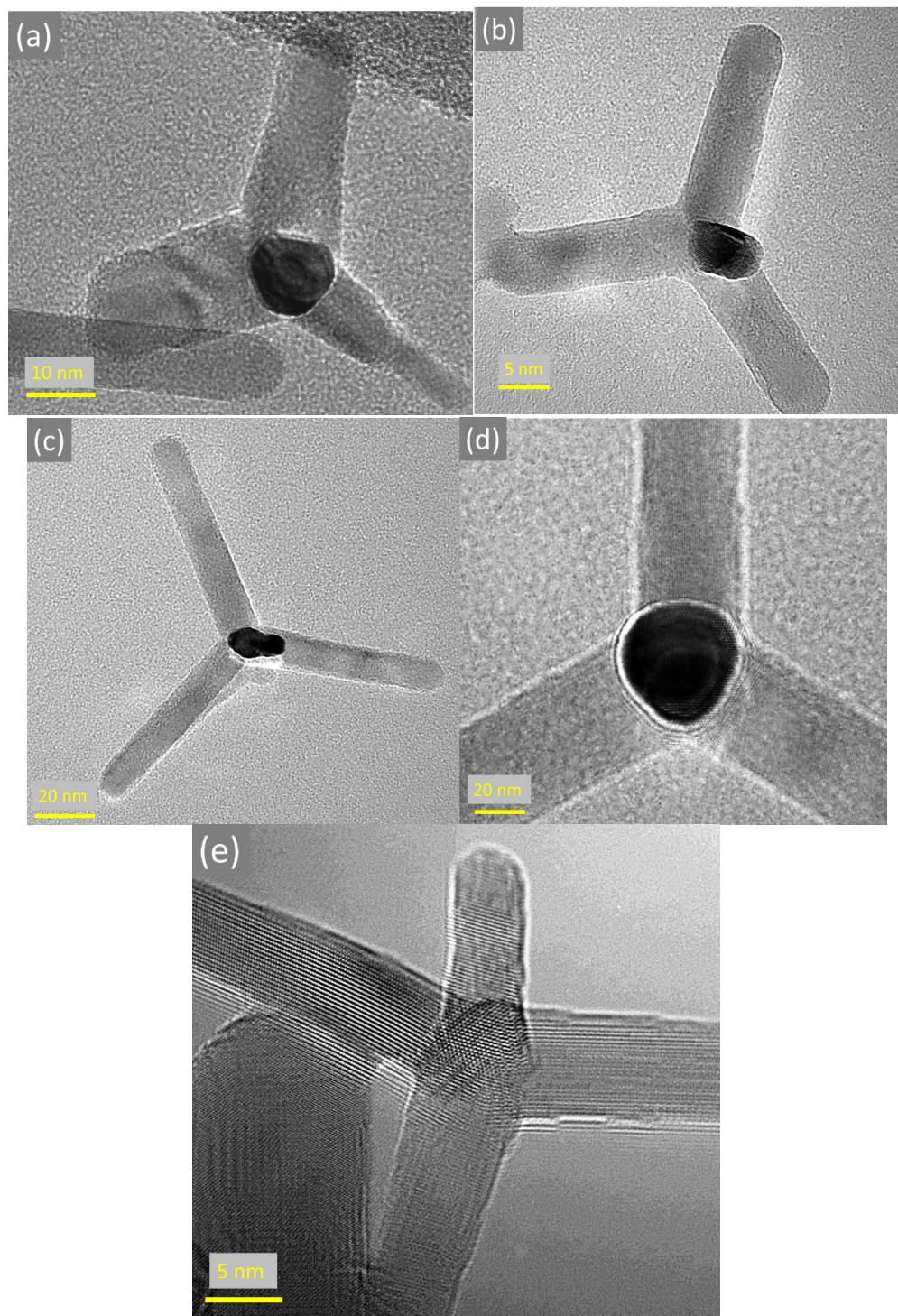


Figure S13. High magnification electron micrograph obtained using TEM for different He gas flows (a) 75 sccm, (b-d)110 sccm and (e)150 sccm at constant 40 W applied RF power.

Reference

- (1) Tauc, J.; Menth, A. States in the Gap. *J. Non. Cryst. Solids* **1972**, *8–10* (C), 569–585. [https://doi.org/10.1016/0022-3093\(72\)90194-9](https://doi.org/10.1016/0022-3093(72)90194-9).
- (2) Bhattacharyya, D.; Chaudhuri, S.; Pal, A. Bandgap and Optical Transitions in Thin Films from Reflectance Measurements. *Vacuum* **1992**, *43* (4), 313–316. [https://doi.org/10.1016/0042-207X\(92\)90163-Q](https://doi.org/10.1016/0042-207X(92)90163-Q).
- (3) Hassanien, A. S.; Akl, A. A. Effect of Se Addition on Optical and Electrical Properties of Chalcogenide CdSSe Thin Films. *Superlattices Microstruct.* **2016**, *89* (January), 153–169. <https://doi.org/10.1016/j.spmi.2015.10.044>.
- (4) Kayaci, F.; Vempati, S.; Donmez, I.; Biyikli, N.; Uyar, T. Role of Zinc Interstitials and Oxygen Vacancies of ZnO in Photocatalysis: A Bottom-up Approach to Control Defect Density. *Nanoscale* **2014**, *6* (17), 10224–10234. <https://doi.org/10.1039/C4NR01887G>.
- (5) Djurišić, A. B.; Leung, Y. H. Optical Properties of ZnO Nanostructures. *Small* **2006**, *2* (8–9), 944–961. <https://doi.org/10.1002/smll.200600134>.
- (6) Cross, R. B. M.; Souza, M. M. De; Narayanan, E. M. S. A Low Temperature Combination Method for the Production of ZnO Nanowires. *Nanotechnology* **2005**, *16* (10), 2188–2192. <https://doi.org/10.1088/0957-4484/16/10/035>.
- (7) Liu, X.; Wu, X.; Cao, H.; Chang, R. P. H. Growth Mechanism and Properties of ZnO Nanorods Synthesized by Plasma-Enhanced Chemical Vapor Deposition. *J. Appl. Phys.* **2004**, *95* (6), 3141–3147. <https://doi.org/10.1063/1.1646440>.
- (8) Yang, Q.; Tang, K.; Zuo, J.; Qian, Y. Synthesis and Luminescent Property of Single-Crystal ZnO Nanobelts by a Simple Low Temperature Evaporation Route. *Appl. Phys. A* **2004**, *79* (8), 1847–1851. <https://doi.org/10.1007/s00339-004-2939-9>.
- (9) Kumar, V.; Gohain, M.; Kant, R.; Ntwaeborwa, O. M.; Hari, P.; Swart, H. C.; Dutta, V. Annealing Induced Oxygen Defects on Green Sonochemically Synthesized ZnO Nanoparticles for Photoelectrochemical Water Splitting. *ChemistrySelect* **2018**, *3* (42), 11914–11921. <https://doi.org/10.1002/slct.201802668>.
- (10) Yu, W.; Li, X.; Gao, X. Catalytic Synthesis and Structural Characteristics of High-Quality Tetrapod-Like ZnO Nanocrystals by a Modified Vapor Transport Process. *Cryst. Growth Des.* **2005**, *5* (1), 151–155. <https://doi.org/10.1021/cg049973r>.
- (11) Liu, Y.; Liu, A.; Liu, W.; Hu, Z.; Sang, Y. Characterization of Optoelectronic Properties of the ZnO Nanorod Array Using Surface Photovoltage Technique. *Appl. Surf. Sci.* **2010**, *257* (4), 1263–1266. <https://doi.org/10.1016/j.apsusc.2010.08.040>.
- (12) Bayan, S.; Mohanta, D. Effect of 80-MeV Nitrogen Ion Irradiation on ZnO Nanoparticles: Mechanism of Selective Defect Related Radiative Emission Features. *Nucl. Instruments Methods Phys. Res. Sect. B Beam Interact. with Mater. Atoms* **2011**, *269* (3), 374–379. <https://doi.org/10.1016/j.nimb.2010.11.044>.

- (13) Zhao, J.-H.; Liu, C.-J.; Lv, Z.-H. Photoluminescence of ZnO Nanoparticles and Nanorods. *Optik (Stuttg.)*. **2016**, *127* (3), 1421–1423. <https://doi.org/10.1016/j.ijleo.2015.11.018>.
- (14) Biesinger, M. C.; Lau, L. W. M.; Gerson, A. R.; Smart, R. S. C. Resolving Surface Chemical States in XPS Analysis of First Row Transition Metals, Oxides and Hydroxides: Sc, Ti, V, Cu and Zn. *Appl. Surf. Sci.* **2010**, *257* (3), 887–898. <https://doi.org/10.1016/j.apsusc.2010.07.086>.
- (15) Tseng, Z.; Chiang, C.; Wu, C. Surface Engineering of ZnO Thin Film for High Efficiency Planar Perovskite Solar Cells. *Sci. Rep.* **2015**, *5* (1), 13211. <https://doi.org/10.1038/srep13211>.
- (16) Zhang, X.; Qin, J.; Xue, Y.; Yu, P.; Zhang, B.; Wang, L.; Liu, R. Effect of Aspect Ratio and Surface Defects on the Photocatalytic Activity of ZnO Nanorods. *Sci. Rep.* **2015**, *4* (1), 4596. <https://doi.org/10.1038/srep04596>.
- (17) Han, X.; He, H.; Kuang, Q.; Zhou, X.; Zhang, X.; Xu, T.; Xie, Z.-X.; Zheng, L.-S. Controlling Morphologies and Tuning the Related Properties of Nano/Microstructured ZnO Crystallites. *J. Phys. Chem. C* **2009**, *113* (2), 584–589. <https://doi.org/10.1021/jp808233e>.
- (18) Senthilkumar, K.; Senthilkumar, O.; Morito, S.; Ohba, T.; Fujita, Y. Synthesis of Zinc Oxide Nanoparticles by Dc Arc Dusty Plasma. *J. Nanoparticle Res.* **2012**, *14* (10), 1205. <https://doi.org/10.1007/s11051-012-1205-x>.
- (19) Pedersen, J. D.; Esposito, H. J.; Teh, K. S. Direct Synthesis and Characterization of Optically Transparent Conformal Zinc Oxide Nanocrystalline Thin Films by Rapid Thermal Plasma CVD. *Nanoscale Res. Lett.* **2011**, *6* (1), 568. <https://doi.org/10.1186/1556-276X-6-568>.
- (20) Zhang, X.-H.; Xie, S.-Y.; Jiang, Z.-Y.; Zhang, X.; Tian, Z.-Q.; Xie, Z.-X.; Huang, R.-B.; Zheng, L.-S. Rational Design and Fabrication of ZnO Nanotubes from Nanowire Templates in a Microwave Plasma System. *J. Phys. Chem. B* **2003**, *107* (37), 10114–10118. <https://doi.org/10.1021/jp034487k>.
- (21) Barreca, D.; Bekermann, D.; Comini, E.; Devi, A.; Fischer, R. A.; Gasparotto, A.; Maccato, C.; Sberveglieri, G.; Tondello, E. 1D ZnO Nano-Assemblies by Plasma-CVD as Chemical Sensors for Flammable and Toxic Gases. *Sensors Actuators B Chem.* **2010**, *149* (1), 1–7. <https://doi.org/10.1016/j.snb.2010.06.048>.
- (22) Jian-Feng, Y.; You-Ming, L.; Hong-Wei, L.; Yi-Chun, L.; Bing-Hui, L.; Xi-Wu, F.; Jun-Ming, Z. Growth and Properties of ZnO Nanotubes Grown on Si(111) Substrate by Plasma-Assisted Molecular Beam Epitaxy. *J. Cryst. Growth* **2005**, *280* (1–2), 206–211. <https://doi.org/10.1016/j.jcrysgro.2005.03.045>.
- (23) Lin, Y.; Tang, Z.; Zhang, Z.; Yuan, F.; Ling, Y.; Lee, J.; Huang, S. Preparation of Nanometer Zinc Oxide Powders by Plasma Pyrolysis Technology and Their Applications. *J. Am. Ceram. Soc.* **2000**, *83* (11), 2869–2871. <https://doi.org/10.1111/j.1151-2916.2000.tb01649.x>.

- (24) Tong, D. G.; Wu, P.; Su, P. K.; Wang, D. Q.; Tian, H. Y. Preparation of Zinc Oxide Nanospheres by Solution Plasma Process and Their Optical Property, Photocatalytic and Antibacterial Activities. *Mater. Lett.* **2012**, *70*, 94–97. <https://doi.org/10.1016/j.matlet.2011.11.114>.
- (25) Tong, D. G.; Luo, Y. Y.; Chu, W.; Guo, Y. C.; Tian, W. Cutting of Carbon Nanotubes via Solution Plasma Processing. *Plasma Chem. Plasma Process.* **2010**, *30* (6), 897–905. <https://doi.org/10.1007/s11090-010-9262-3>.
- (26) Park, J.-S.; Park, D.-W. Synthesis of Zinc Oxide Nano-Particles Using Carbon Dioxide by DC Plasma Jet. *Surf. Coatings Technol.* **2010**, *205* (SUPPL. 1), S79–S83. <https://doi.org/10.1016/j.surfcoat.2010.04.046>.
- (27) Ananth, A.; Dharaneedharan, S.; Seo, H. J.; Heo, M. S.; Boo, J. H. Soft Jet Plasma-Assisted Synthesis of Zinc Oxide Nanomaterials: Morphology Controls and Antibacterial Activity of ZnO. *Chem. Eng. J.* **2017**, *322*, 742–751. <https://doi.org/10.1016/j.cej.2017.03.100>.
- (28) Peng, H.; Fangli, Y.; Liuyang, B.; Jinlin, L.; Yunfa, C. Plasma Synthesis of Large Quantities of Zinc Oxide Nanorods. *J. Phys. Chem. C* **2007**, *111* (1), 194–200. <https://doi.org/10.1021/jp065390b>.
- (29) Liao, S.-C.; Lin, H.-F.; Hung, S.-W.; Hu, C.-T. Dc Thermal Plasma Synthesis and Properties of Zinc Oxide Nanorods. *J. Vac. Sci. Technol. B Microelectron. Nanom. Struct. Process. Meas. Phenom.* **2006**, *24* (3), 1322–1326. <https://doi.org/10.1116/1.2197513>.
- (30) Schwan, A. M.; Chwatal, S.; Hendler, C.; Kopp, D.; Lackner, J. M.; Kaindl, R.; Tscherner, M.; Zirkl, M.; Angerer, P.; Friessnegger, B.; Augl, S.; Heim, D.; Hinterer, A.; Stummer, M.; Waldhauser, W. Morphology-Controlled Atmospheric Pressure Plasma Synthesis of Zinc Oxide Nanoparticles for Piezoelectric Sensors. *Appl. Nanosci.* **2023**, *13* (9), 6421–6432. <https://doi.org/10.1007/s13204-023-02936-w>.
- (31) Bilik, N.; Greenberg, B. L.; Yang, J.; Aydil, E. S.; Kortshagen, U. R. Atmospheric-Pressure Glow Plasma Synthesis of Plasmonic and Photoluminescent Zinc Oxide Nanocrystals. *J. Appl. Phys.* **2016**, *119* (24). <https://doi.org/10.1063/1.4954323>.
- (32) Zhang, C.; Geng, X.; Li, H.; He, P.-J.; Planche, M.-P.; Liao, H.; Olivier, M.-G.; Debliquy, M. Microstructure and Gas Sensing Properties of Solution Precursor Plasma-Sprayed Zinc Oxide Coatings. *Mater. Res. Bull.* **2015**, *63*, 67–71. <https://doi.org/10.1016/j.materresbull.2014.11.044>.
- (33) Parlakyigit, A. S.; Ergun, C.; Gokcekaya, O. Synthesis of ZnO Nanoparticles via Spray Atomization Assisted Inductively Coupled Plasma Technique. *Ceram. Int.* **2023**, *49* (14), 23035–23044. <https://doi.org/10.1016/j.ceramint.2023.04.129>.